JOURNAL OF GEOPHYSICAL RESEARCH, VOL. 105, NO. C6, PAGES 14,237–14,251, JUNE 15, 2000

Bathymetry, stratification, and internal seiche structure

P. D. Fricker and H. M. Nepf

Department of Civil and Environmental Engineering, Ralph M. Parsons Laboratory, Massachusetts Institute of Technology, Cambridge

Abstract. Internal seiches play a significant role in a broad range of physical, chemical, and biological processes in lakes. A detailed assessment of the impact of seiching requires an understanding of seiche structure, which is determined by bathymetry and stratification. In this study, internal seiche solutions are evaluated for arbitrary bathymetry and continuous stratification using a two-dimensional numerical model. Formulated in terms of a stream function, the model produces a finite set of linear internal wave eigenmodes and allows the computation of the complete velocity field (over a grid) associated with each seiche mode. Several idealized configurations of continuous stratification and variable bathymetry are used to explore the effect of nonuniform systems on internal wave structure. In particular, we focus on bed velocity distribution and the resulting potential impact on scalar fluxes, sediment transport, and internal wave damping. Model results are also compared to thermistor chain data collected in the Upper Mystic Lake (UML, Winchester, Massachusetts). Using an idealized description of the UML bathymetry and density profiles which emulate the seasonal variation of stratification in the lake, the evolution of bed velocities during the autumnal breakdown in stratification is assessed, providing insight into the fate of the contaminants entering the lake.

1. Introduction

Internal seiches play a significant role in a broad range of physical, chemical, and biological processes in lakes. By mediating exposure to light and nutrients, the vertical excursions of fluid associated with the wave motions have been shown to affect the spatial distribution of macroscopic and microscopic organisms [*Levy et al.*, 1991; *Haury et al.*, 1983]. The sustained oscillations of water over the bed contribute to the generation of a benthic boundary layer, which enhances the dissolution, resuspension, and transport of nutrients, contaminants, and sediment [*Gloor et al.*, 1994; *Pierson and Weyhenmeyer*, 1994], and contribute to effective vertical mixing through horizontal buoyancy-driven flows [*Ivey and Corcos*, 1982; *Heinz et al.*, 1990]. For example, *MacManus and Duck* [1988] showed that seiche-induced resuspension was responsible for the sediment scouring patterns observed along the sides of Loch Earn. Because of the lake's relatively simple shape, they were able to model the spatial (i.e., nodal) properties of the seiches using a simple rectangular basin model. Assessing the impact of seiching in lakes with more complex bathymetry is more difficult because the internal seiches themselves are modified by the basin. In the present study we use a numerical method to evaluate the internal seiches in lakes with nonuniform bathymetry and stratification, focusing attention specifically on the V1H1-type mode. The principal objectives of this work are to examine the effect of bathymetry and stratification on seiche structure and ultimately to determine the potential impact of seiche motions on resuspension and dissolution of bed material.

Since the earliest studies of internal seiching, the spatial characteristics and oscillation periods of individual internal wave modes have been evaluated using simplified analytical formulations. Lakes were originally modelled as rectangular basins with a two-layer density profile [e.g., *Wedderburn*, 1907, 1912; *Heaps and Ramsbottom*, 1966]. A principal drawback to this formulation is that it can only describe the first vertical mode (i.e. V1Hn, $n = 1, 2, ...$). This can be a serious limitation because higher vertical modes, particularly V2H1, are now known to be present in many systems [*LaZerte*, 1980; *Wiegand and Chamberlain*, 1987; *Münnich et al.*, 1992].

Increased computing power has allowed the development of progressively more sophisticated models of internal seiching. The advances in modelling have generally fallen into two categories: improved descriptions of stratification and the generalization to arbitrary bathymetry. With regard to the former, wave modes for a continuous stratification were computed numerically by *Csanady* [1968a, b], *Birchfield* [1969], and *Monismith* [1987] and pseudoanalytically by *Csanady* [1972] as one-dimensional eigenvalue problems in an idealized rectangular or cylindrical basin. *Csanady* [1982] and *Monismith* [1985] also used a multiple-layer matrix formulation to approximate continuous density profiles.

Paper number 2000JC900060.
0148-0227/00/2000JC900060$09.00

Although these models yield improved estimates of internal seiche period, they do not provide a realistic picture of spatial structure, owing to the use of oversimplified bathymetries. Conversely, most models which incorporate a more accurate basin shape use an overly simplistic two-layer density profile. For example, methods such as the two-layer Defant procedure (TDP), which is an adaptation by *Mortimer* [1979] and *Lemmin and Mortimer* [1986] of a surface seiche model [*Defant*, 1918, 1961], as well as the two-layer variable depth (TVD) model [*Schwab*, 1977; *Horn et al.*, 1986], only describe vertical internal seiche motion in the horizontal plane at the interface.

In the present study, internal seiches are evaluated for systems with both irregular bathymetry and realistic continuous stratification, using a two-dimensional numerical eigenvalue technique. The method can be considered a generalization to two dimensions of the procedure used by *Csanady* [1968a, b], *Birchfield* [1969], and *Monismith* [1987] described above. A similar eigenvalue method was first used by *Wang and Yih* [1976] to investigate waves in a basin with semicircular bathymetry. However, their analysis was performed for a two-layer fluid, and discussion was therefore restricted to horizontal modes. More recently, *Münnich* [1996] studied the effect of varying topography on internal seiches using a formulation similar to that presented here, but only considered uniform stratification.

As a test case, internal seiche solutions are computed for the Upper Mystic Lake (UML, Winchester, Massachusetts). Thermistor chain data have been collected in the UML for several field seasons as part of an ongoing investigation of the mobilization of contaminants in the system. These data allow direct comparison between the model results and real internal seiche behavior. The Mystic Lake bathymetry is comprised of a deep main basin and a shallow shelf which extends over one third of the lake. This feature is typical of many systems; lakes with similar bathymetries, although larger in scale, include Lakes Geneva and Zürich. Many of the results presented here are therefore directly applicable to these systems.

The model results demonstrate that large-scale bathymetric features lead to the magnification of flow at specific locations along the bed. The resulting spatially nonuniform bed stress will give rise to enhanced localized mixing in the benthic boundary layer, which in turn can cause localized increases in nutrient and contaminant fluxes due to both resuspension and enhanced dissolution. For the UML bathymetry the model shows that the velocities on the shelf are substantially magnified, even when the mixed layer is very shallow and the thermocline region is relatively high above the bed. Furthermore, as the position of the thermocline varies seasonally, the modification of the internal waves due to the bathymetry also changes, with the greatest magnification of flow occuring as the bottom of the surface mixed layer approaches the depth of the shelf.

2. Numerical Method

Internal seiche solutions are evaluated for arbitrary bathymetry and continuous stratification using a two-dimensional (2-D) numerical model. Formulated in terms of a stream function, the model produces a finite set of linear internal wave eigenmodes, which allows the computation of the complete displacement and velocity field (over a grid) associated with each seiche mode.

A linearized governing equation for internal waves in two dimensions can be derived from the full (2-D) inviscid momentum (Euler) equations and continuity. The pressure (P) and density (ρ) are decomposed into mean and perturbation fields,

$$\begin{aligned} P(x,z,t) &\rightarrow \overline{P}(z) + P'(x,z,t) \\ \rho(x,z,t) &\rightarrow \overline{\rho}(z) + \rho'(x,z,t) \end{aligned} \quad , \tag{1}$$

with the perturbation terms corresponding to the seiche motion (velocity field $\mathbf{q}(x,z,t) = (u,w)$). In the momentum equations, the mean pressure and density are found to satisfy the hydrostatic relation

$$\overline{P}_z = g\overline{\rho}$$

and therefore cancel one another. In this expression and throughout the paper, we use the notation $f_x \equiv \partial f/\partial x$.

In the usual way, the velocity field may be expressed in terms of a stream function,

$$u = \psi_z \qquad w = -\psi_x \quad , \tag{2}$$

which can be summarized as $\mathbf{q} = (u,w) = \boldsymbol{\nabla} \times \boldsymbol{\Gamma}$, with $\boldsymbol{\Gamma} \equiv (0,\psi,0)$. Since we seek wave solutions, we assume oscillatory behavior in the perturbation fields, i.e.,

$$\phi(x,z,t) \Rightarrow \Re\left[\phi(x,z)e^{i\omega t}\right] \quad ,$$

where $\phi = (\psi, \rho', P')$. Neglecting nonlinear terms, which is valid for small wave amplitudes, this formulation yields the governing equation [see, e.g., *Yih*, 1980, p. 70]

$$\psi_{zz} - \frac{N^2}{g}\psi_z - \frac{N^2 - \omega^2}{\omega^2}\psi_{xx} = 0 \quad , \tag{3}$$

where $N^2(z) = -\frac{g}{\rho}\overline{\rho}_z$ is the buoyancy frequency. The boundary conditions that complete this system are found from the no-flux requirement on the velocities:

$$\mathbf{n}\cdot\mathbf{q} = 0 \quad \rightarrow \quad \mathbf{n}\cdot(\boldsymbol{\nabla}\times\boldsymbol{\Gamma}) = \mathbf{p}\cdot\boldsymbol{\nabla}\psi = 0 \quad , \tag{4}$$

where $\mathbf{n}$ and $\mathbf{p}$ are unit vectors normal to and parallel with the boundary, respectively (i.e., $\mathbf{n}\cdot\mathbf{p} = 0$). Since $\mathbf{p}\cdot\boldsymbol{\nabla}\psi = \partial\psi/\partial s$ is zero everywhere along the boundary, denoted by coordinate s, we are free to take $\psi(s) = 0$ without loss of generality. Finally, for simplicity we also make the rigid lid approximation and set $\psi(x,0) = 0$.

Other than linearization and the rigid lid, no additional approximations were made in this derivation. Additional simplifications are possible, however, the most common being the hydrostatic and Boussinesq approximations. For example, *Thorpe* [1968] presented an analysis of higher-order nonlinear expansion terms for progressive internal waves, using the zeroth–order solution in a Boussinesq fluid. *Münnich* [1996] numerically evaluated linear eigenmodes using both approximations. The resulting governing equation,

$$\psi_{zz} - \frac{N^2}{\omega^2}\psi_{xx} = 0 \quad , \tag{5}$$

has the advantage that the eigenvalues vary linearly with the dimensions of the system and are, in that sense, scale-independent. The principle benefit of this is that round-off errors in the computations can be avoided, which might otherwise result from the small vertical-to-horizontal aspect ratio in the discretization of a real lake system. The possibility of round-off error does arise when working with (3) and may lead to a steppiness in the computed solutions. For the systems we consider, the hydrostatic and Boussinesq terms are exceptionally small and could justifiably be neglected. However, since the inclusion or omission of these terms has no impact on the difficulty or tractability of the problem in our calculations, we have no need to exclude them. We therefore employ (3) for all the analyses.

For a nonregular basin, (3) is not separable, and the eigensolutions for the full 2-D system must be evaluated numerically. The equation may be rewritten as

$$N^2\psi_{xx} = \omega^2\left(\psi_{zz} - \frac{N^2}{g}\psi_z + \psi_{xx}\right) \quad , \tag{6}$$

which, along with the boundary conditions, are discretized such that the matrix formulation of the problem has the generalized eigenvalue form,

$$\mathbf{N}\Psi = \omega^2\mathbf{M}\Psi \quad .$$

$\mathbf{N}$ denotes a matrix whose elements are determined in part by the buoyancy frequency (the left-hand side of (6)), while $\mathbf{M}$ corresponds to the discretization of the right-hand side. If either of the matrices $\mathbf{M}$, $\mathbf{N}$ has an inverse, which is generally the case, then (6) can be put in standard eigenvalue form. In the present study, the problem is solved in standard form using a finite difference formulation.

The velocities are evaluated by taking derivatives of the numerical stream function solution (see (2)). In general, grid points in the computational mesh do not lie on the boundary but instead are located a fractional distance from the bed, in both the x and z directions. To improve the estimate of velocity at the bed, the numerical solution is interpolated over a finer grid, exploiting the known condition $\psi(s) = 0$, to generate data closer to the boundary (s). A slight steppiness is still observed in the final result, but this effect can be arbitrarily minimized by using an even finer grid. To compare the model results to thermistor chain observations, we calculate the vertical fluid displacements,

$$\zeta = -\frac{1}{i\omega}\psi_x \quad , \tag{7}$$

which only differ from the vertical velocities by the factor $(i\omega)^{-1}$. This factor will be ignored, since we are interested in the envelope of the seiche motion and not the absolute magnitude.

The eigensolutions which correspond to the fundamental modes, for example the V1H1 or V2H1 analogues, appear mid-way within the manifold of computed solutions to (6). In other words, their eigenvalues are neither the largest nor the smallest in the solution set. The reason for this is illustrated by the analytical solution to (3) for a rectangular basin and constant N^2 (e.g. Turner, 1973, page 23):

$$\psi(x,z) = \psi_0 \sin\frac{n\pi x}{L} e^{-\frac{N^2}{2g}z} \sin\frac{m\pi z}{H} \quad , \tag{8}$$

in which the horizontal and vertical mode numbers ($n, m = 1, 2, 3, ...$) are related to the frequency by

$$\frac{\omega_{nm}^2}{N^2} = \frac{n^2}{n^2 + \mu^{-2}m^2 + \frac{N^4L^2}{4\pi^2g^2}} \quad , \tag{9}$$

where $\mu = \frac{H}{L}$. The maximum and minimum values of ω_{nm} correspond respectively to $n \to \infty$ and $m \to \infty$, with the other mode number bounded. The seiche modes of greatest interest, for which $n \approx m \approx 1$, do not correspond to an extremum eigenvalue. As a result, it is necessary to compute all of the eigensolutions for the discretized system and then identify the desired oscillations from among the entire set by inspection, using their nodal properties. This makes the analysis computationally expensive, thereby limiting the possible size of the discretization. However, the structural features of the numerical seiche solutions presented in this paper were generally found to be unaffected by the size of the discretization employed. In most of the computations, the square domain overlying the basin was discretized in a 40×40 grid, resulting in 1045 wet points (and 1045×1045 matrices) for the parabolic basin and 869 wet points for the model UML basin. A 30×30 grid was used for the series which included the largest (nearly rectangular) basin, owing to the prohibitive size of the resulting matrices.

Lastly, the use of a 2-D model in this study raises the issue of attempting a three-dimensional (3-D) formulation. While a 3-D formulation is possible (in terms of the seiche-related pressure deviation field $P'(x,y,z,t)$), it was found to be prohibitively difficult for the following three reasons: (1) Adding an extra dimension generates larger matrices and hence a larger eigenvalue computation. (2) The eigenvalue problem is quadratic (and is also complex), requiring that the size of the matrix system be doubled in order to reduce it to a linear form. (3) The boundary conditions for the system are Neumann conditions, so that the resulting matrices tend to be singular. This means that the eigenvalue problem cannot be recast in standard form and must be solved as a more expensive generalized problem. Fortunately, the 2-D formulation presented here provides meaningful results for longitudinal seiches in small to mid-sized lakes, for which Coriolis effects are unimportant. The excellent agreement between model results and field observations supports this conclusion, as demonstrated in section 3.

3. Test Case: The Upper Mystic Lake

3.1. Site Description

The Upper Mystic Lake (UML, Figure 1) is located in greater metropolitan Boston, at the southern end of the Aberjona Watershed. The lake is relatively small, roughly 1000 m long and 600 m wide, with a maximum depth of 25 m.

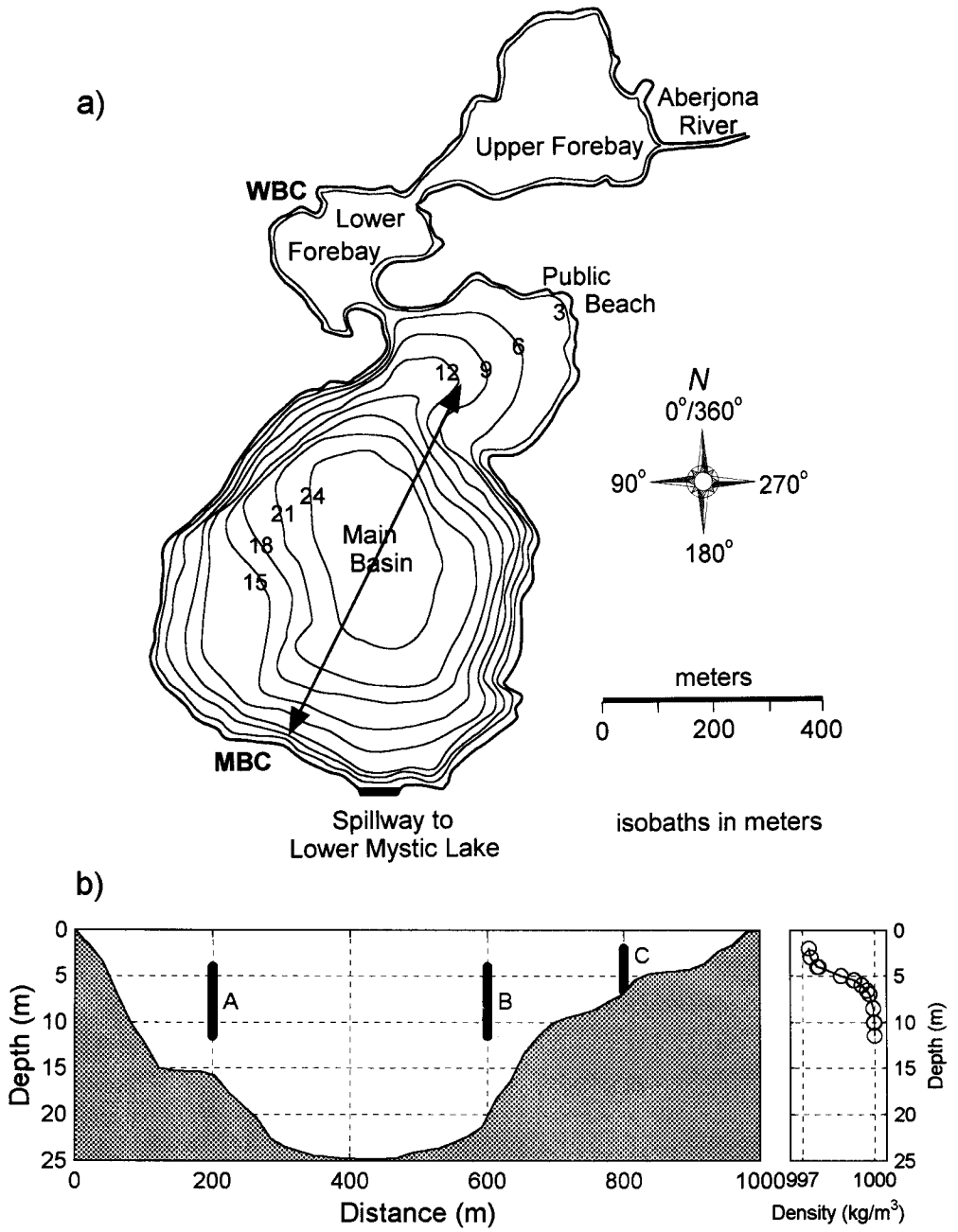

Figure 1. (a) The Upper Mystic Lake (Winchester, Massachusetts), with depth contours plotted in 3 m increments. The positions of the thermistor chains are labeled A, B, and C, and the predominant wind-forcing axis (oriented at ~ 340°/160°) is denoted by the solid arrow. (b) The bathymetry of the UML along the wind axis, with projections of the approximate locations of the thermistor chains. Wind data were collected at the Medford Boat Club (MBC) at the southern end of the lake.

The principal axis of wind forcing is almost aligned with the major axis of the lake (also shown in Figure 1), with winds predominantly from the south in summer and from the north in winter. This is due to a combination of local ambient weather conditions and the presence of low hills which flank the UML on its eastern and western sides. Stratification conditions at midsummer are consistently strong, with typical surface and bottom temperatures of 27°-30°C and 5°-6°C, respectively, and a surface layer depth of roughly 4 m. The bathymetric cross section along the major axis (Figure 1b) shows that the northern third of the lake consists of a shoal with maximum depth 9 m. The stratification profile shown at the right is derived from thermistor chain data collected in late summer. Later results will show that the location of the thermocline relative to the shelf has a major impact on the internal seiches in the lake.

The Aberjona Watershed is highly contaminated with organic and metal industrial wastes, the legacy of an industrial

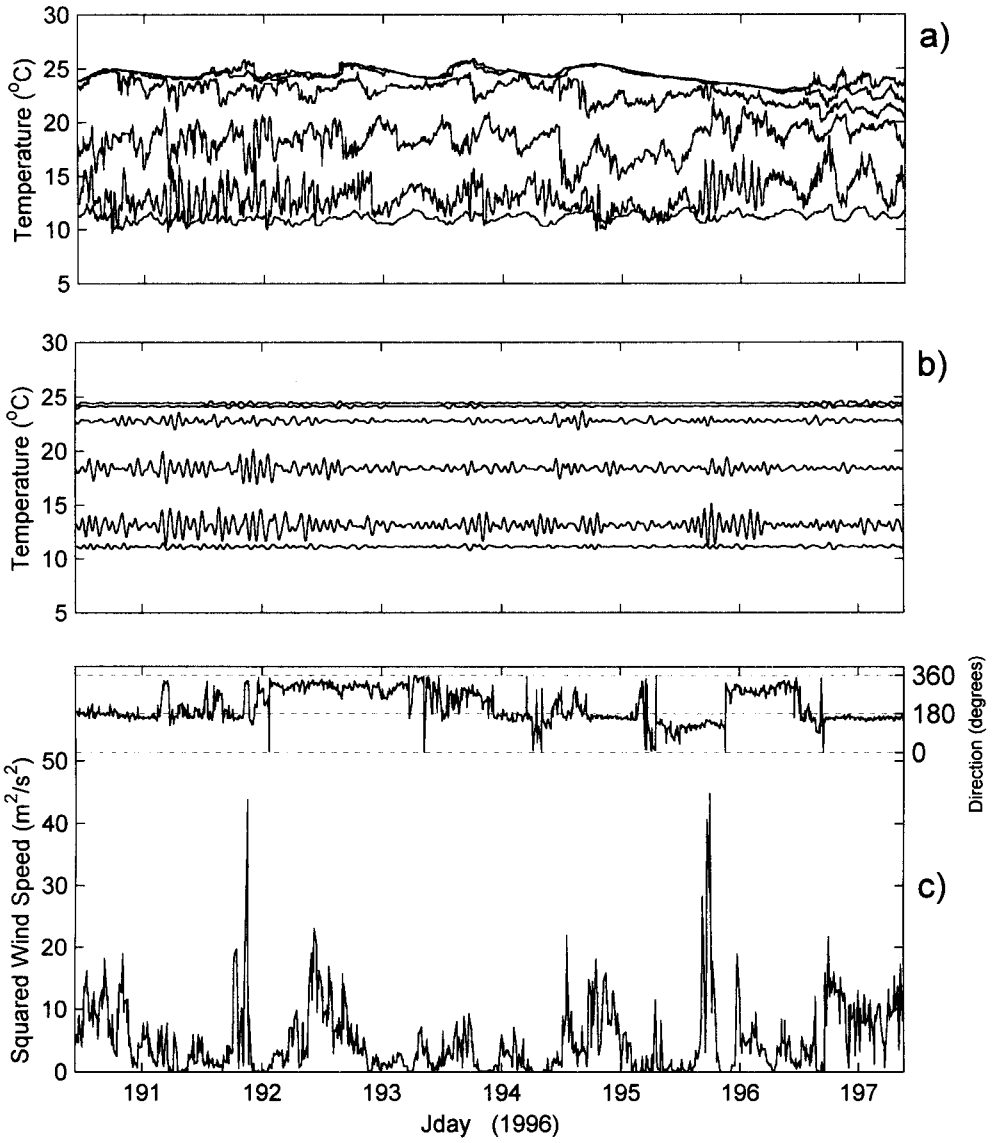

Figure 2. A sample of temperature data from thermistor chain C in the UML. (a) Raw data for a 7-day period in July 1996. The bottom thermistor in the chain was resting on the lake bed, giving rise to a damped signal. (b) The same temperature record as Figure 2a, after band-pass filtering (0.3-0.9 cph) around the V1H1 internal seiche period (0.6 cph). (c) The simultaneous wind record, measured at the southern end of the UML. The wind direction is plotted in the inset at the top of Figure 2c; 0° is North.

period which spanned ~150 years [*Durant et al.*, 1990; *Spliethoff and Hemond*, 1996]. The Aberjona river continues to bring contaminants such as arsenic, chromium, and lead into the Mystic Lake system at a rate of hundreds of kilograms per year (150 kg/yr As, for example; *Solo-Gabriele*, [1995]). Chemical studies of the UML have found concentrations of As and Cr of the order of 5 g/kg in the sediments [*Spliethoff and Hemond*, 1996] and As concentrations up to 0.1 μM in the water column [*Trowbridge*, 1995]. The objective of the present study is to assess the potential contribution of internal seiching to the fluxes of contaminants in the UML. In particular, we investigate how the seasonal variation of seiche structure, especially at the bed, can lead to a temporal variation in these fluxes.

3.2. Data Collection and Analysis

Temperature data were collected in the UML using thermistor chains at three locations (labeled A, B, and C in Figure 1). Each chain consisted of six thermistors, with vertical spacings of 1.5 m for the chains at A and B and 1.0 m at C. On the basis of previous studies [*Trowbridge*, 1995; *Aurilio et al.*, 1994], and using an understanding of typical midsummer stratification conditions in the UML, the thermistors at A and B were placed to span an optimal region of the thermocline for observing seiche motions, running from the bottom of the surface mixed layer (~4 m) to a depth of nearly 12 m. Below this depth the density gradient becomes sufficiently small that estimates of seiche amplitude based on thermistor records are unreliable. Chain C was located in the

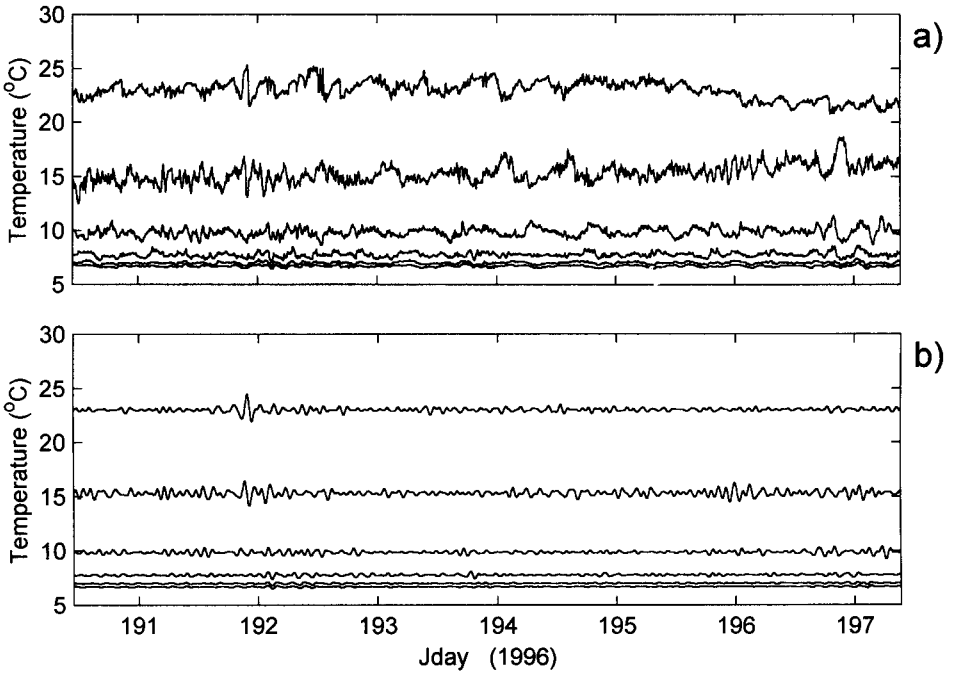

Figure 3. Thermistor data at chain A, for the same time period shown in Figure 2. (a) Raw data. (b) The data in Figure 3a, after band-pass filtering (0.3-0.9 cph).

shallower part of the lake and was therefore placed higher in the water column, from 2 m to ~6.5 m in depth. After deployment the bottom thermistor was found to be lying on the sediment. The exact depth of each system was determined using a pressure transducer mounted on the datalogger unit located at the top of each chain. The three systems were placed in a staggered arrangement to allow assessment of three-dimensional seiche motion. However, no transverse or rotational motion was detected in any of the data collected. Although transverse seiching can occur in principle, these modes did not feature in the UML internal wave spectra, most likely because the wind forcing consistently aligns with the major axis of the lake (see Figure 1), as discussed in section 3.1. Temperature measurements were recorded every 5 min. Concurrent wind (speed and direction) measurements were recorded at 10 min intervals by an anemometer placed roughly 12 m above the water surface atop a flag pole, at the Medford Boat Club (MBC) at the southern end of the lake (Figure 1).

Previous thermistor chain studies [*Trowbridge*, 1995] have shown that the V1H1 (~0.6 cph) and V2H1 (~0.09 cph) modes are the dominant seiches in the UML. Since the V1H1 seiche is the focus of the current paper, motion associated with this mode is isolated from the temperature data by filtering around 0.6 cph (band pass 0.3-0.9 cph). A sample of raw and filtered data from chain C (i.e. over the shelf), along with the corresponding wind record, is presented in Figure 2 for a 7-day period in midsummer. The data show both the presence of sustained V1H1 and V2H1 oscillations and the response to a transient forcing event. For example, the strong burst of wind at Jday 195.6 generated a sudden increase in the amplitude of the V1H1 mode. Comparison to the data collected at chain A (Figure 3) shows that this response is substantially greater in the shallow part of the lake (chain C) than in the main basin (chain A), indicating localized magnification of fluid displacement in this region.

Thermistor chain data can be used to identify the internal wave modes present in a lake by matching observed seiche frequencies to model predictions and (for the gravest modes) by comparing the phases of motions recorded at different locations in a lake. However, the overall sparsity of data, particularly in the horizontal, makes it difficult to develop a clear picture of the spatial structure of the seiches. The numerical model, however, provides a description of seiche structure over the entire longitudinal and vertical cross section of the lake. Once the model solutions have been validated through comparison to the field data, they can be used to infer more detailed information about the structure and impact of the seiches.

To determine seiche amplitude from the thermistor data, a mean temperature profile $\overline{T}(z)$ is first constructed by averaging the time series temperature measurements in the selected time period and pooling the data from the three chains (Figure 4). An RMS temperature deviation ΔT_{rms} is then computed for the V1H1 mode from a selected length of filtered thermistor record (N points),

$$\Delta T^{i}_{\mathrm{rms}} \equiv \sqrt{\frac{2}{N}\sum_{n=1}^{N}\left[T(\mathbf{x}_i,t_n)-\overline{T}(\mathbf{x}_i)\right]^2}\ , \qquad (10a)$$

where

$$\overline{T}(\mathbf{x}_i)=\frac{1}{N}\sum_{n=1}^{N}T(\mathbf{x}_i,t_n)\ ,$$

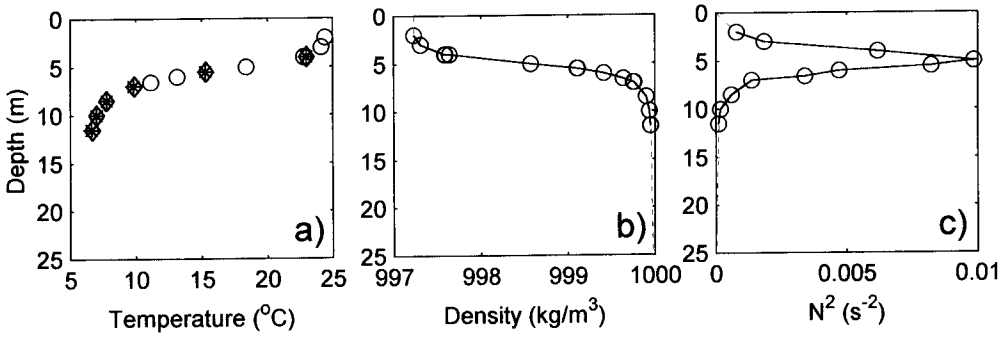

Figure 4. Mean temperature data derived from thermistor chains A, B, and C for the time period shown in figures 3 and 4 (Jday 191-197). (a) Mean temperature at each thermistor on chains A (∗), B (◇), C (o). Chains A and B were positioned at the same depth in the water column. (b) Mean densities at each thermistor, calculated from the data in Figure 4a. The data from the three chains are assembled in a single profile (solid line); the data points at chains A and B are averaged. The profile is extrapolated to the surface and to the bed (dashed lines). (c) Buoyancy frequency profile derived from the temperature data in Figure 4a.

and $\mathbf{x}_i$ denotes the position of thermistor i. The factor of 2 in this expression eliminates the factor of $1/2$ introduced by the summation, which is analogous to period averaging. Finally, RMS seiche amplitudes are determined as

$$\zeta^i_{\mathrm{rms}} = \frac{\triangle T^i_{\mathrm{rms}}}{\partial T/\partial z} \quad , \tag{10b}$$

in which the local gradient $\partial\overline{T}/\partial z$ is estimated from the composite temperature profile (Figure 4). Note that the computed $\triangle T_{\mathrm{rms}}$ profiles represent the envelope of wave motion for the V1 modes only because for these modes the vertical fluid motions at any horizontal location are in phase throughout the water column, and the sign of $\left[T\left(t_n\right) - \overline{T}\right]$ at any instant in time t_n is the same for all the thermistors on each chain. For higher vertical modes, the $\triangle T_{\mathrm{rms}}$ represent the absolute value of the wave envelope. Finally, note in 10b that the RMS temperature deviations are assumed to correspond entirely to vertical fluid motions. In the thermistor chain data, however, horizontal displacements can also contribute to the observed $\triangle T_{\mathrm{rms}}$ at locations where a strong vertical temperature gradient impinges on a sloping boundary. We therefore anticipate a divergence between the observed ζ_{rms} and the simulated ζ near the bed at chain C.

4. Results and Discussion

4.1. Comparison to the Model

The stream function contour plot shown in Figure 5 is the numerically evaluated V1H1 seiche in the UML for the time

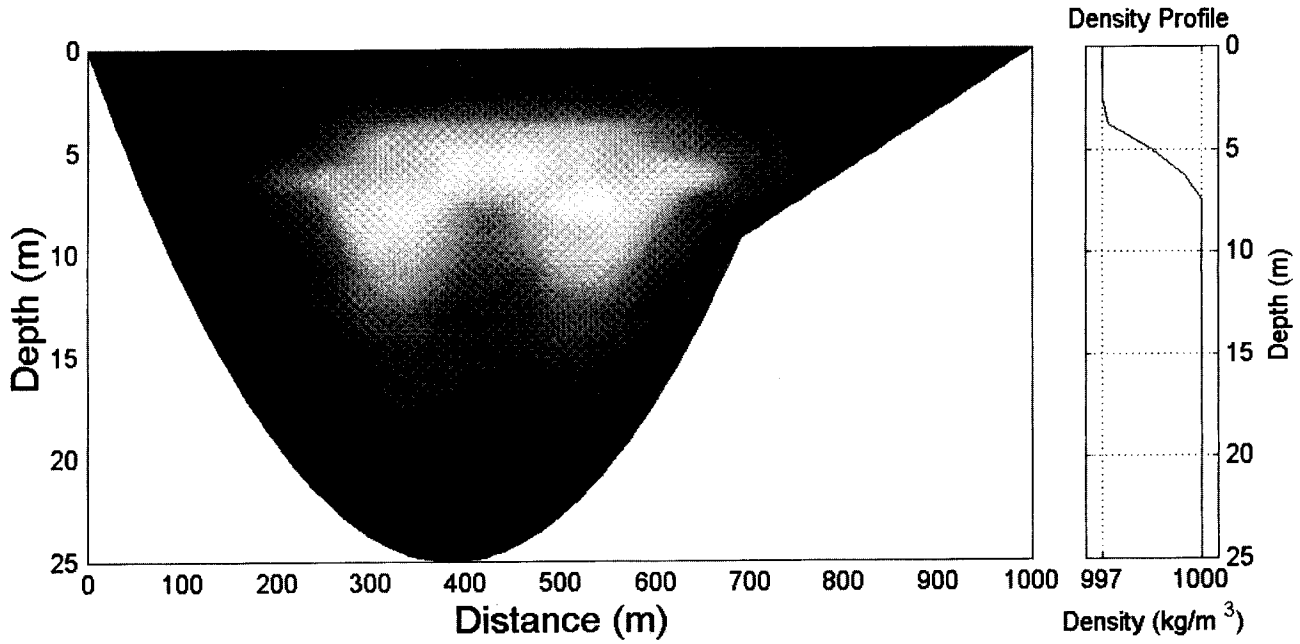

Figure 5. Stream function contours of the simulated V1H1 mode in the UML. The density profile used to generate this solution, shown on the right, is derived from the profile in Figure 4.

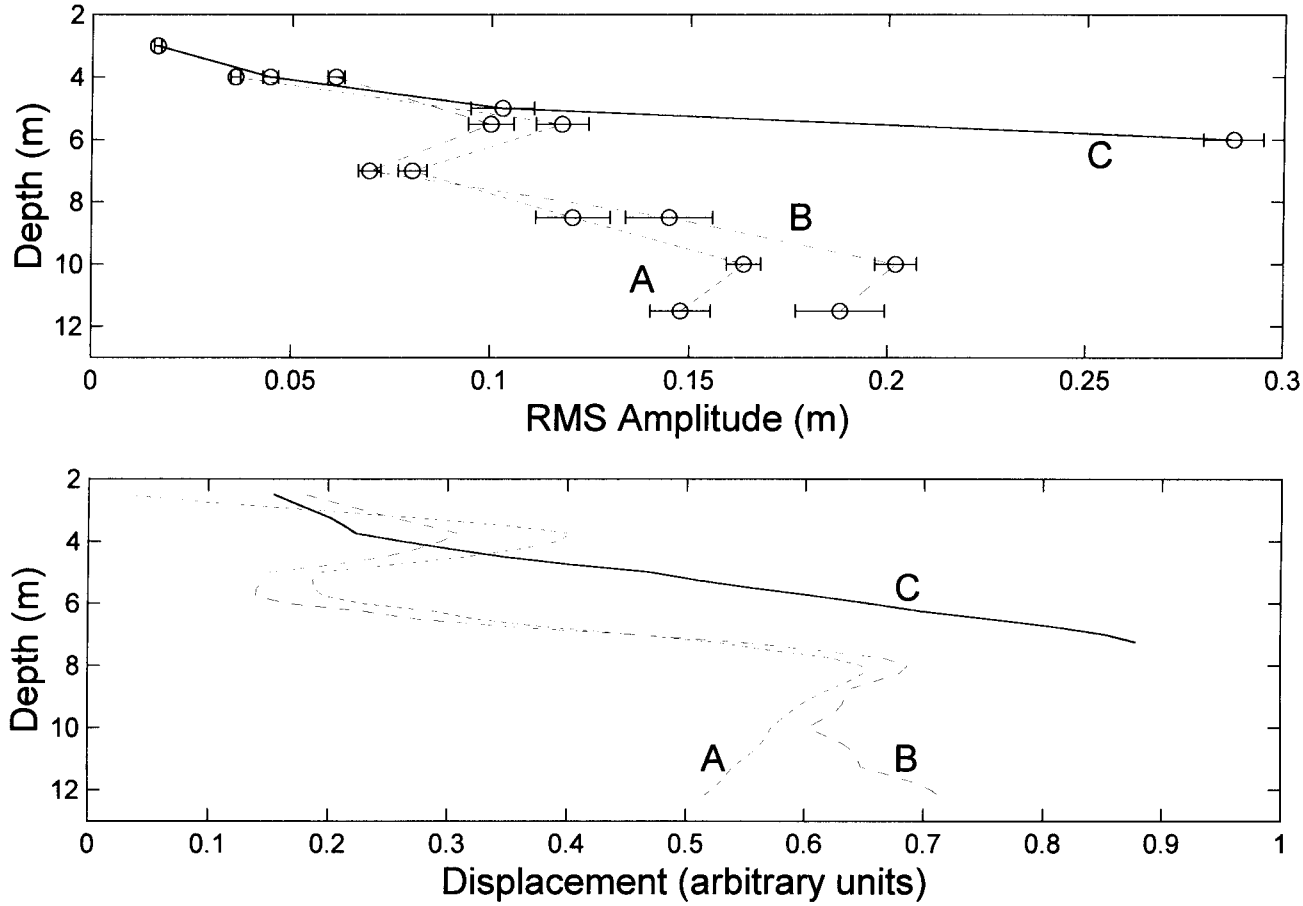

Figure 6. (a) RMS vertical displacements at Chains A, B, and C in the UML, using the data in Figures 2 and 3 for chains C and A, respectively, and the corresponding data for the same time period for chain B. The bars indicate the estimated error, which primarily results from the computation of $\partial T/\partial z$ from the temperature profile. (b) The model simulation, computed from the solution in Figure 5.

period shown in Figure 2 (Jday 191-197). The basin shape used to compute this solution corresponds to the bathymetry along the major axis of the lake (see Figure 1), and the density profile, shown on the right, is an idealization based on the composite temperature profile shown in Figure 4. Simulated vertical profiles of ζ derived from this solution (Figure 5) using (7) are shown in Figure 6 for three longitudinal positions corresponding to the approximate locations of the three thermistor chains (see Figure 1). The model profiles match those from the lake data. For the main basin profiles (A,B) the model correctly predicts two local maxima, one at the base of the surface mixed layer and another at an intermediate depth within the pycnocline. The RMS amplitudes at chain A are slightly greater than those at B for the higher lying peak, while the opposite is true for the deeper peak. The simulated profiles mirror this behavior. Over the shelf, the RMS amplitude at chain C increases down to the bed in both the observed and modeled profiles. The differences in magnitudes directly at the bed probably arise because (10) overpredicts the ζ_{rms} by neglecting the contribution of horizontal motions to the observed temperature variations, as discussed in section 3.2. The differences between the simulations and the data in the vertical positions and magnitudes of the peaks are most likely due to differences between the real lake bathymetry (Figure 1) and the idealization (Figure 5) and to the low spatial resolution of the temperature measurements. Overall these results suggest that the numerical model provides a good description of the structure of the V1H1 internal seiche.

4.2. Stratification and Bed Velocities

To assess the potential impact of seiching on contaminant fluxes and resuspension, we focus on the structure of the V1H1-type seiche at the lake bed. In this section we use a parabolic basin to investigate the relationship between stratification and seiche-related bed velocities. The relative importance of other processes which affect sediment transport, such as river inflow and surface wave action, is not assessed here.

As lakes lose heat in the autumn, the breakdown in stratification can be characterized as a decrease in surface layer temperature and a deepening of both the epilimnion and the pycnocline. During this process, internal seiche structure (and climate) in the lake also changes. Although it was assumed that $\overline{\rho}(z)$ is not a function of time in the derivation of

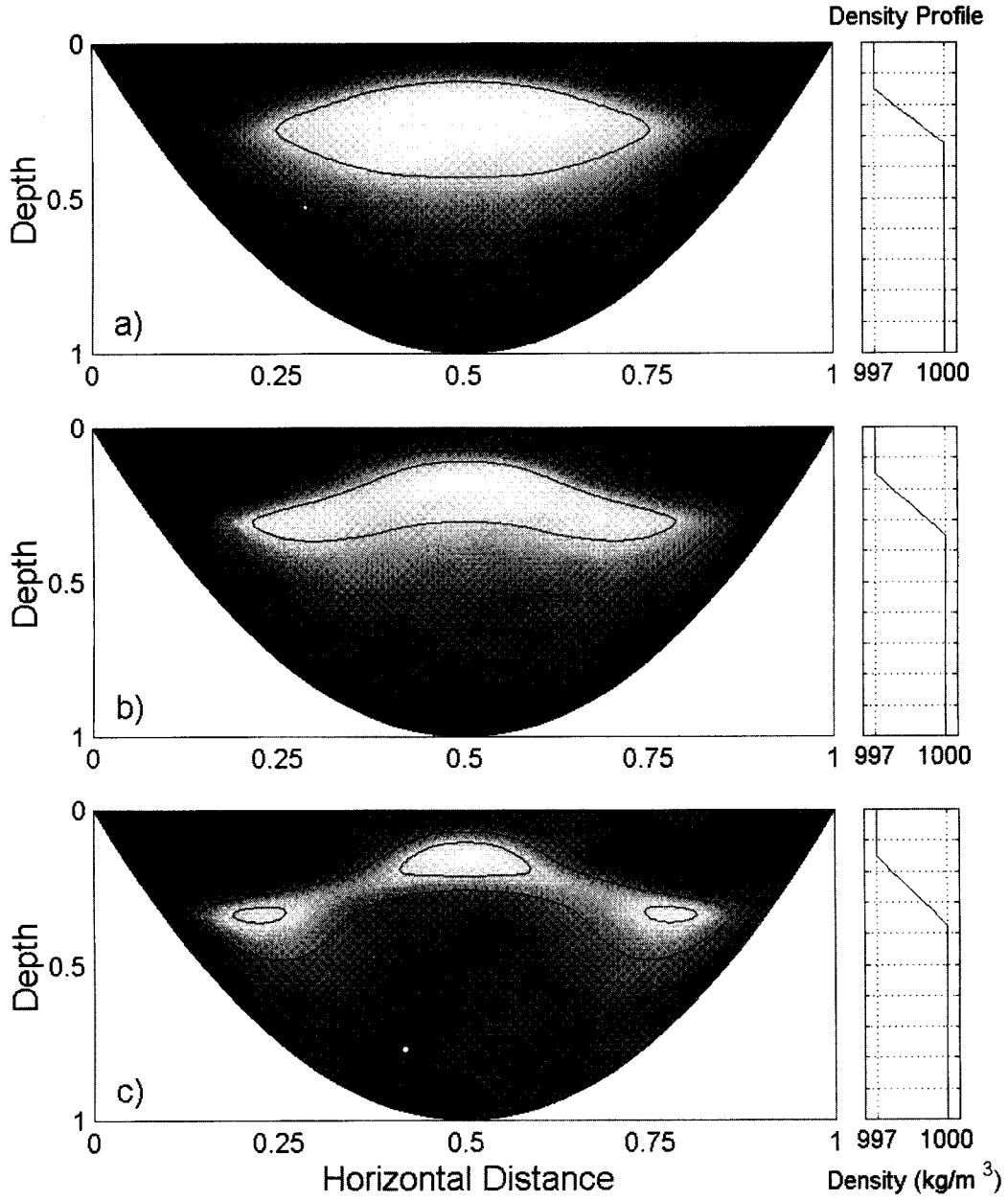

Figure 7. V1H1 seiche solutions evaluated in a parabolic basin. The density profiles used to compute each solution (shown on the right) are comprised of a surface mixed layer with thickness $h_{\text{epi}} = 0.15H$, and a pycnocline region which is broadened sequentially by one grid point ($\triangle z = 1/40H$), from $h_{\text{pyc}} = 0.18H$ to $0.22H$. The lines show the $\psi = 0.25, 0.5, 0.75$ contours.

the governing equation (3), the model may be used for this analysis if the timescale for significant changes in the density profile $\triangle\tau$ ($\sim$10 days) is much longer than the internal wave periods $2\pi\omega^{-1}$;

$$\frac{\nabla\cdot(\overline{\rho}_t\nabla\psi_t)}{\nabla\cdot(\overline{\rho}\nabla\psi_{tt})} \sim \frac{\triangle\overline{\rho}_0/\triangle\tau}{\overline{\rho}_0\omega} \sim \frac{\varepsilon}{\omega\triangle\tau} \ll 1 \ ,$$

where $\varepsilon \equiv \triangle\overline{\rho}_0/\overline{\rho}_0 \sim 0.003$. For modeling purposes, we describe the evolving stratification using a sequence of idealized density profiles comprised of a homogeneous epilimnion and hypolimnion connected by a linearly varying pycnocline (see Figure 7, for example). These profiles can be parameterized in terms of the thicknesses of the epilimnion (h_{epi}) and pycnocline (h_{pyc}) and by the surface and hypolimnion densities. In this analysis we focus on the impact of changing layer thicknesses on seiche structure. Changes in surface temperature have a direct impact on seiche frequency but only weakly affect seiche structure (of the order of the Boussinesq approximation) and are not considered here.

Figure 7 shows a series of V1H1 seiche solutions evaluated in a parabolic basin ($h\,(x) = 1 - (2x-1)^2$) for three different density profiles. Recall that the governing equation

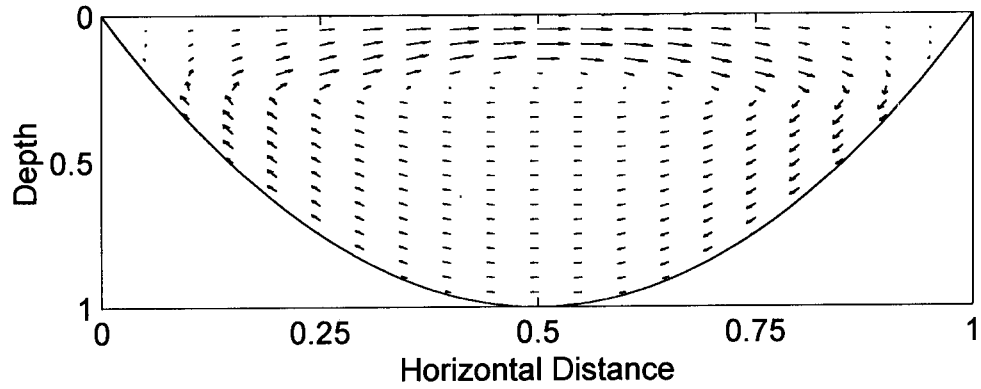

Figure 8. Velocity field derived from the V1H1 streamfunction solution in Figure 7a (see equation (2)). The solution is computed for a 40×40 grid but presented on a 20×20 grid for clarity.

(3) is not scale-independent (section 2). In order to have the magnitudes of the Boussinesq and hydrostatic terms be of correct order, it is necessary to use a vertical-to-horizontal aspect ratio which is typical of real lakes. The calculations are performed using the UML dimensions ($H = 25$ m, $L = 1000$ m) and densities ($\overline{\rho}(0) = 997$ kg/m^3 and $\overline{\rho}(H) = 1000$ kg/m^3), but the solutions are presented in normalized spatial coordinates. All of the solutions in Figure 7 were computed for an epilimnion depth of $h_{\text{epi}} = 0.15H$. The pycnocline thickness is broadened sequentially by one grid point ($\triangle z = 1/40$), with $h_{\text{pyc}} = 0.18H$, $0.20H$, and $0.22H$ for Figures 7a, 7b, and 7c respectively. The profiles are denoted ρ_1, ρ_2, and ρ_3 for convenience.

To demonstrate the connection between these stream function solutions and the more familiar velocity field, u and w are computed for the solution in Figure 7a and plotted in Figure 8. The plot represents the spatial envelope of a standing wave, with the arrows reversing direction sinusoidally in time with the seiche frequency. This solution corresponds to the V1H1 mode in the rectangular basin. As this example illustrates, the V1H1 analogue can be identified in more complex basins by the absence of nodes (i.e., changes in sign) in the stream function contours in either the horizontal or vertical direction.

The bed velocity distributions for the three solutions in Figure 7 are shown in Figure 9 (solid lines, labeled ρ_1, ρ_2, and ρ_3), along with three additional curves. The fourth solid line (ρ_{2L}) is the two-layer solution for $h_{\text{epi}} = 0.15H$. The dashed curves represent the two-layer solutions for epilimnion thicknesses of $h_{\text{epi}} = 0.25H$ and $0.35H$ and will be discussed below. In all cases the U_{bed} are normalized by the total energy of the seiche,

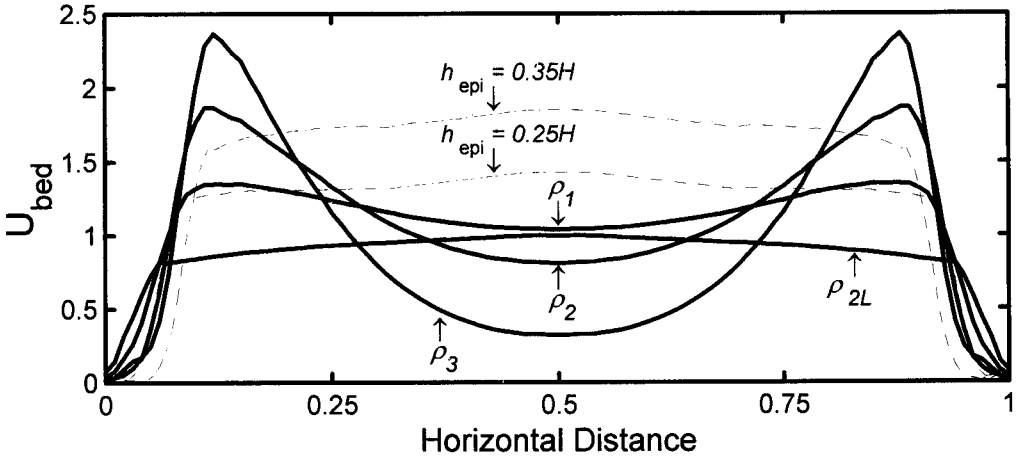

Figure 9. Bed velocities derived from the solutions in Figure 7, plus three additional solutions. To generate the curves, the stream function contours were first interpolated onto a finer grid and then used to compute $q_{\text{bed}} = \sqrt{u_{\text{bed}}^2 + w_{\text{bed}}^2}$ using equation (2). Residual steppiness was smoothed with five-point averaging. The curves were normalized as in equation (11) and then rescaled by the maximum value of the ρ_{2L} solution. The solid lines were all computed with $h_{\text{epi}} = 0.15H$ and show the evolution of bed velocity with increasing pycnocline thickness ($h_{\text{pyc}} = 0$ (ρ_{2L}), $0.18H$ (ρ_1), $0.2H$ (ρ_2), $0.22H$ (ρ_3)). The dashed lines were computed using two-layer density profiles ($h_{\text{pyc}} = 0$), with $h_{\text{epi}} = 0.25H$ and $0.25H$. Along with the ρ_{2L} solution, these curves show the changes in U_{bed} with increasing epilimnion depth.

$$U_{\text{bed}} \equiv \frac{q_{\text{bed}}}{\sqrt{2E/\rho_0 V}} \qquad q_{\text{bed}} = \sqrt{u_{\text{bed}}^2 + w_{\text{bed}}^2} \ , \quad (11)$$

where the total mass is

$$\rho_0 V \equiv \int_V \overline{\rho} dx dz \ ,$$

and where (due to equipartition of energies)

$$E = |E_{\text{kin}}| = \frac{1}{2} \int_V \overline{\rho} \left(u^2 + w^2\right) dx dz \qquad (12)$$

to allow direct comparison among the six cases. They are then rescaled to set the midlake maximum of the ρ_{2L} curve to unity, for convenience in illustrating the magnification of the flow. The velocity structures shown in Figure 9 clearly differ from rectangular basin solutions, for which U_{bed} ($\sim \sin \pi x/L$) has a maximum at the center of the lake regardless of stratification. For the parabolic basin considered here, the maximum U_{bed} only occurs at mid-lake when the pycnocline is exceptionally thin, as the two-layer solution shows (ρ_{2L}). As the pycnocline thickness increases, U_{bed} makes the transition to the two-peaked profiles seen for $\rho_1 - \rho_3$. Making the simple assumption that sediment is scoured from regions of high bed velocity and deposited in locations of lower bed velocity, the off-center maxima imply that sediment will be carried not just toward the "edges" of the lake but also toward the center. Furthermore, moving from ρ_1 to ρ_3 (i.e., increasing h_{pyc}), we see a substantial increase in the maximum value of U_{bed} around $x = 0.1$ and 0.9 and a dramatic decrease in velocity at midlake as the bottom of the lake is progressively cut off from the seiche motion. In fact, the results in Figure 9 suggest that there is a density profile for which U_{bed} at the center of the lake drops to zero. In this respect, the bed velocity structures in the (more realistic) parabolic basin differ substantially from the corresponding rectangular basin solutions for these stratification profiles.

To estimate the damping rate for the internal seiches, we assume that the seiche energy is dissipated predominantly through bed shear. The E defined in (12) is the energy (per unit width) for an inviscid system and is therefore constant over time. If we assume that the viscous damping of the seiches has small magnitude, we can permit a small transient component to E and estimate the dissipation of energy using a first-order model,

$$\frac{dE}{dt} = -kE \ .$$

This is then balanced by the work done at the bed (coordinate s):

$$-kE = \int_\partial \tau_{\text{bed}} U_{\text{bed}} ds \ .$$

The bed stress can be taken as $\tau_{\text{bed}} = \overline{\rho} C_b U_{1m}^2$ (i.e., U at 1m) with $C_b = 0.005$ [*Dimai et al.*, 1994]. Using the bed velocities in Figure 9 as representative of U_{1m}, we then find

$$k = \frac{C_b \int_\partial \overline{\rho} U_{\text{bed}}^3 ds}{\int_V \overline{\rho} \left(u^2 + w^2\right) dx dz} \ . \qquad (13)$$

Table 1. Damping coefficients for the density profiles in Figure 9.

Profile	k/k_{2L}
$\rho 2L$	1.0
$\rho 1$	2.4
$\rho 2$	3.4
$\rho 3$	3.4
$0.25H$	2.0
$0.35H$	5.0

The relative damping coefficients for each of the six cases is shown in Table 1. Each k is normalized by the two-layer ($h_{\text{epi}} = 0.15$) solution. We see that the damping rate for the seiches increases four-fold as the metalimnion is broadened and the bed velocities at the base of the pycnocline increase. Likewise, for the two-layer profiles, as the interface moves closer to the bed, we see a substantial increase in k. These results illustrate the effect of internal seiche structure on energy dissipation and show that the attenuation of the seiching is controlled in part by stratification and bathymetry. This clearly has an impact on the seasonal variation in seiche activity.

Returning to Figure 7, note that the seiche develops a ray-like structure as the thickness of the pycnocline increases (ρ_1 to ρ_3). Figure 7c in particular suggests that the model system is approaching a critical behavior, with the seiche energy confined to a narrow conduit within the water column, i.e., along the stream function contours. As described below, this transition from coherent seiche to energy focusing is consistent with the wave ray analysis of *Maas and Lam* [1995]. For uniform stratification (constant N), they concluded that for most bathymetries the internal wave rays (i.e., energy) generated within the lake become focused along specific lines, called attractors, and that coherent internal seiches only form in a limited number of basins. One such bathymetry is the bucket shape, comprised of a flat bed with linear sloping side walls. For the systems we consider ($N \approx$ constant in the pycnocline and $N = 0$ in the surface and lower layers), when the pycnocline is thin, the shape of the "waveguide" region in which the wave rays can propagate approximates the bucket-shaped basin, with slightly rounded sides. Although these two configurations are not exactly equivalent (because they have different boundary conditions; the BC $\psi = 0$ applies at the free surface and the bed, not at the boundary of the pycnocline), the geometric similarity strongly suggests a correspondence between their seiche solutions. When the pycnocline widens, the shape of the waveguide region becomes less bucket-like, and focusing behavior begins to emerge, as the progression in Figure 7 shows. In addition, in our numerical calculations, as h_{pyc} is increased further, beyond that in ρ_3 by one or more additional grid points, the system makes the full transition to wave ray focusing, and we no longer obtain smooth V1H1 solutions such as those in Figure 7. This is also consistent with the conclusions of *Maas*

and Lam [1995], who suggest that systems which are subject to focusing are poorly described by discretization methods. It is not possible to make a direct comparison between the cases considered here (i.e., profiles for which focusing does not occur and coherent seiche solutions are found) and the results of Maas and Lam, however, since these authors only considered uniform stratification.

Regarding the above observation of an apparent approach toward a critical behavior, viscous and nonlinear processes, which were omitted from the present formulation, will likely prevent this behavior from occuring in real systems (as *Maas and Lam* [1995] also note in their analysis). Specifically, as the seiche energy becomes more focused and velocities are increasingly magnified, nonlinearity and viscosity become important and lead to greater damping. This can be seen from the results above (Table 1), in which the increases in h_{pyc} led to a four-fold increase in the decay rate k. The impact of nonlinear terms can be inferred from the curves in Figure 9; as U_{bed} increases at the base of the pycnocline, the advective terms $\sim U_{\mathrm{bed}}\partial U_{\mathrm{bed}}/\partial s$ grow substantially.

Along with the ρ_{2L} curve, the dashed lines in Figure 9 show the evolution of bed velocities with changing surface layer depth, h_{epi}. Two-layer density profiles were used in these calculations to isolate the changes in bed velocity structure due to increasing h_{epi}. The trends were found to be qualitatively similar for all values of h_{pyc}. As the epilimnion deepens, the bed velocities show a steady increase in the deepest part of the lake. This result is easily explained using a simple depth-averaged perspective. As the thickness of the lower layer decreases, conservation of mass requires that the flow at the bottom of the lake increases relative to the upper layer, $u_2 = -h_1/h2\, u_1$. Normalizing by the system energy then gives $|u_2|\,/\sqrt{E/\rho_0 V} = \sqrt{2h_1/h2}$, which predicts increases in $|u_2|$ ($\sim |U_{\mathrm{bed}}|$) of 40 and 75% as h_{epi} is increased from $0.15H$ to $0.25H$, respectively, and from $0.15H$ to $0.35H$. These increases are very close to the results in Figure 9.

We conclude by noting that the 2-D model used in the present study effectively reduces to the method of *Wang and Yih* [1976] when a two-layer stratification is used. Therefore the results in Figure 9 (i.e., the qualitative and quantitative differences between the two-layer and ρ_1, ρ_2, ρ_3 curves) also illustrate some of the differences between two-layer models and the numerical technique used here (with continuous stratification). For example, the magnification of U_{bed} associated with the development of a ray-like seiche structure clearly cannot occur in two-layer systems. Figure 9 thus demonstrates the importance of an accurate description of vertical structure and of the limitations of a two-layer perspective.

4.3. Bathymetry and Bed Velocities

In this section we investigate the dependence of bed velocities on bathymetry, using a series of basins ranging from rectangular to parabolic. The bathymetry in each case is given by

$$h(x) = \frac{\cosh\alpha - \cosh\alpha\,(2x-1)}{\cosh\alpha - 1}$$

(for which $h(0) = h(1) = 0$, $h\left(\frac{1}{2}\right) = 1$) and is parametrized in terms of the variable α, which corresponds to an index of concavity. The two extreme basin shapes are given by $\alpha \to 0$ (parabola $h(x) \to 1 - (2x-1)^2$) and $\alpha \to \infty$ (rectangle). The density profile is the same as the profile in Figure 7a.

Figure 10 shows the bed velocity profiles computed for six configurations ($\alpha = 100, 10, 5, 3, 2, 1$). The corresponding basin shapes are also shown. The U_{bed} are once again normalized as described in (10), and then rescaled to set the mid-lake maximum U_{bed} of the rectangular basin solution to unity. Moving from $\alpha = 100$ (~rectangular) to $\alpha = 1$ (~parabolic), a region of substantially enhanced velocities develops at two locations, where the base of the pycnocline reaches the bed. While U_{bed} at the center of the lake decreases by 20 per cent, the velocities at $x \simeq 0.1$ and 0.9 increase by approximately a factor of 5, ultimately becoming as much as 50 percent greater than U_{bed} at mid-lake. We anticipate substantially different sedimentation patterns for each of the six cases. In particular, for the nearly rectangular bathymetry, the observed distribution of U_{bed} will tend to carry sediment away from the center of the lake, causing a build-up at the "corners" of the basin. For the parabola, however, the off-center maxima cause sediment to be carried both toward the edges of the lake and to the center. Furthermore, for the same total seiche energy, the scouring is greatest in the metalimnion region of the parabolic basin because the highest bed velocities are generated in that system.

4.4. Seasonal Variation of Bed Velocities in the UML

Because of the high level of contaminants in the sediments of the UML, the enhanced benthic mixing, dissolution, and transport associated with the internal seiches can be an important factor contributing to the water quality of the lake. Also, because the seiches vary seasonally (in structure and climate), their contribution to contaminant (and nutrient) fluxes will also vary with time. In this section we assess the temporal changes in bed velocity for the V1H1 seiche arising from the autumnal changes in stratification in the UML.

Bed velocities for three different stratification profiles are shown in Figure 11 (solid lines). The representation of the UML bathymetry (dashed line) which was used to compute these solutions is laid over the velocity curves. The velocities are again normalized by the total seiche energy (equation (11)), and subsequently rescaled by the overall maximum value of the three solutions. The density profiles are comprised of a surface mixed layer, a linearly varying pycnocline, and a homogeneous hypolimnion (Figure 11, inset), and represent an idealization of the autumnal breakdown in stratification, based on profiles measured on August 21, October 13, and November 4 in 1992 [*Aurilio et al.*, 1994]. When the pycnocline is relatively high in the water column (August 21), the region of magnified flow extends over a

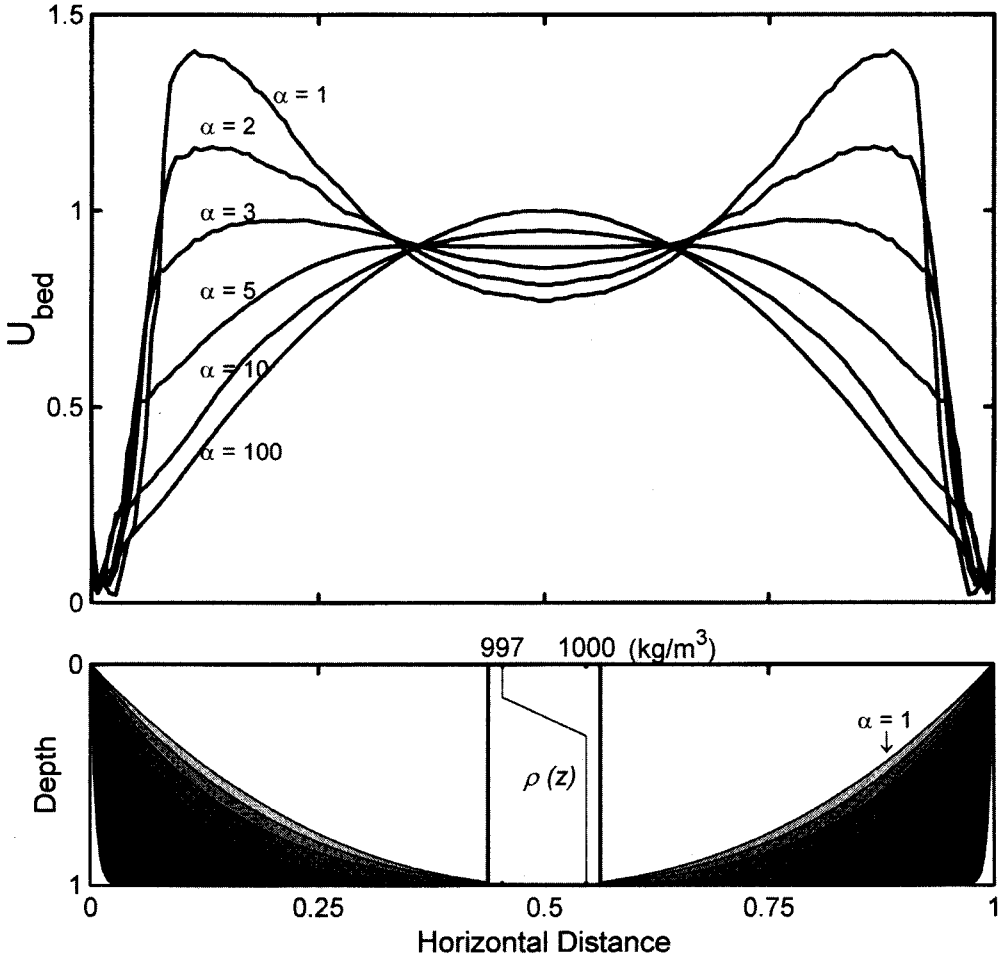

Figure 10. (a) Bed velocity versus horizontal distance for six basins of varying concavity ($\alpha = 1, 2, 3, 5, 10, 100$). (b) The corresponding bathymetries. The curves were generated and processed the same way as those in Figure 9 and then rescaled by the maximum (i.e., midlake) value for the rectangular basin soution ($\alpha \rightarrow \infty$).

broad region of the shoal in the northern end of the lake (right side of Figure 11). As the lake cools and the mixed layer deepens (October 13), the maximum amplitude of U_{bed} remains essentially unchanged, but the region of amplified flows becomes localized to a much narrower region of the shelf. This suggests that the fluid further up on the shelf becomes disconnected from the seiching motion. Finally, when the lake cools still further and the pycnocline drops below the level of the shelf (November 4), the amplified flows over the shelf disappear, and an increase in main basin flows is observed. At this point the entire shelf is disconnected from seiche-induced flows.

The observed temporal evolution of the maximum U_{bed} and the migration of the magnified flow region can play significant roles in the annual influx of contaminants to the UML. Metal-laden sediments enter the system from a river inlet near the northern end of the lake (Figure 1b, right side), arriving first at the shelf. The seasonal strong winds that begin in the autumn coincide with the changes in U_{bed} described above in this section. Although an exact prediction of the magnitude of the V1H1 seiche (or indeed any seiche) requires specific information about wind forcing, we nonetheless know qualitatively that the V1H1 seiche is strongly excited in the UML during the fall. We therefore conclude that the bed motions outlined in Figure 11 may have a substantial impact on the initial deposition and subsequent mobilization of contaminants in the lake. Future field studies of sediments in the UML will explore the link between seiching and sediment distribution.

5. Conclusions

The results presented here show that internal seiche structure is highly dependent on both bathymetry and stratification. Simpler lake models which use a rectangular basin and/or two-layer stratification formulation, which are frequently used for convenient characterizations of seiche motion, provide poor descriptions of even the basic qualitative features of seiches. For example, the V1H1 vertical motions observed and modeled in the UML differ substantially from

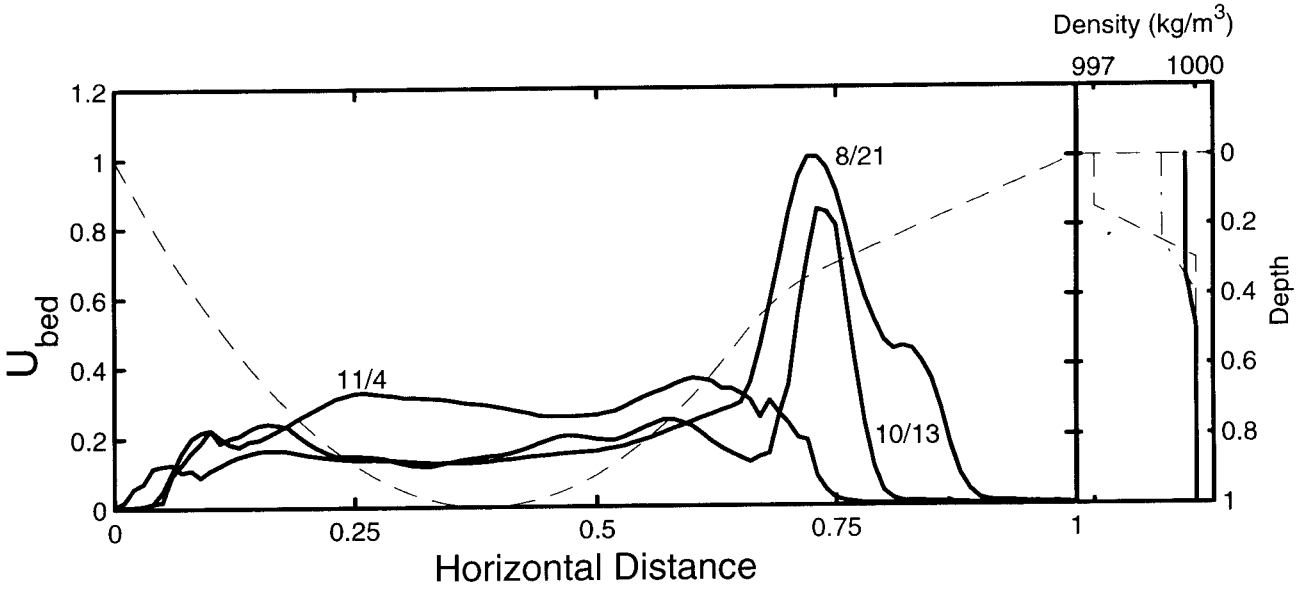

Figure 11. Bed velocities for three different density profiles which simulate the seasonal evolution of stratification in the UML [from *Aurilio et al.*, 1994]; the curves are labeled with the dates on which the density profiles were measured. The idealized density profiles used to generate these solutions are shown in the inset figure, and the model UML bathymetry used in the computations is also shown (dashed line). The data were generated the same way as in Figures 9 and 10 but rescaled in this case by the maximum overall value on the data set (August 21 curve at $x \simeq 0.75$).

rectangular basin structure functions. The accurate modeling of seiches therefore requires the use of realistic density profiles and basin shapes.

In this paper we have assessed the effects of bathymetry and stratification on seiche structure. A 2-D numerical model was used to compute a finite set of seiche eigensolutions in systems with variable bathymetry and continuous stratification. Each solution yields a description of the entire velocity or displacement field of the seiche and can thus be used to augment the extremely limited spatial information provided by thermistor chain data. The model can therefore be a valuable tool for interpreting field observations. In addition, the entire set of computed eigenmodes can also be used as a basis for describing the composition of internal seiche data, both in the field and from hydrodynamic model simulations.

The dependence of seiche structure on stratification was investigated using a series of density profiles in a parabolic basin. The results show that the depth of the epilimnion (h_{epi}) and the thickness of the pycnocline (h_{pyc}) affect both the magnitude and the distribution of bed velocities. The observed variation in U_{bed} as a function of h_{epi} is easily explained by conservation of (horizontal) volume flux throughout the water column. The dependence of U_{bed} on h_{pyc} is somewhat more complicated, however. Except for cases where the pycnocline is exceptionally sharp (tending to a discrete interface), the maximum bed velocities occur where the base of the pycnocline intersects the bed, and the center of the lake corresponds to a local minimum in U_{bed}. Furthermore, as the pycnocline thickness increases, the U_{bed} maxima are magnified while the velocity at midlake drops toward zero, and the deepest part of the lake becomes cut off from the seiching motion. The net effect of this evolution in bed velocities is an increase in the damping rate of the seiches (k) with increasing h_{pyc}. This is in complete contrast to the rectangular basin model results, which predict a single velocity maximum at midlake for the V1H1 mode (i.e., $U \propto \sin \pi x/L$) for all stratification conditions. This implies that basin shape also plays an important role in determining seiche structure. The dependence on bathymetry was confirmed by computing the V1H1 seiche solutions for a single density profile in a series of basins of varying concavity. As the basin shape was changed from rectangular to parabolic, the computed U_{bed} evolved smoothly from the single midlake maximum curve into the two-peaked distribution described above. By altering the magnitude and spatial distribution of the boundary shear, the basin shape influences the long-term fate of sediments and the damping of internal seiche motion.

Application of the model to the UML demonstrated the potential impact on bed velocities of the autumnal stratification breakdown. The most important consequence of the changing conditions in the lake is the migration of the magnified bed-flow region. During the summer the maximum bed velocity peak is located on the shelf and is relatively broad. Moving into the fall, as the surface layer deepens and the pycnocline begins to broaden, the region of elevated velocity narrows. Ultimately, as the base of the pycnocline deepens and drops below the shoal, the flows over the shelf disappear altogether. This variation in U_{bed} has potentially important consequences for the transport of contaminants in the UML. Contaminant-laden sediment entering the lake is initially deposited over the shelf. The timing and magnitude

of the remobilization of these contaminants depend strongly on the bed velocities over the shelf and therefore on the spatial structure and temporal evolution of the seiche.

Acknowledgments. The authors gratefully acknowledge the help of the Winchester Boat Club, which made its facilities, and some of its members, available for the deployment of equipment and the routine collection of data. We also thank the Medford Boat Club for providing a site for wind data collection. We thank Hrund Andradóttir, Gordon Ruggaber, and Enrique Vivoni for their help deploying the thermistor chains and anemometer. Helpful comments from Ole Madsen regarding interpretation of the data were greatly appreciated. This research was funded by NIEHS, grant P42-ES04675.

References

Aurilio, A. C., R. P. Mason, and H. F. Hemond, Speciation and fate of arsenic in three lakes of the Aberjona Watershed, *Env. Sci. Technol. 28*(4), 577-585, 1994.

Birchfield, G. E., Response of a circular model great lake to a suddenly imposed wind stress, *J. Geophys. Res., 74*, 5547-5554, 1969.

Csanady, G. T., Wind-driven summer circulation in the Great Lakes, *J. Geophys. Res. 73*, 2579-2589, 1968a.

Csanady, G. T., Motions in a model Great Lake due to a suddenly imposed wind, *J. Geophys. Res., 73*, 6435–6447, 1968b.

Csanady, G. T., Response of large stratified lakes to wind. *J. Phys. Oceanogr., 2*, 3–13, 1972.

Csanady, G. T., On the structure of transient upwelling events, *J. Phys. Oceanogr., 12*, 84-96, 1982.

Defant, A., Neue Methode zur Ermittlung der Eigenschwingungen von abgeschlossenen Wassermassen, *Ann. Hydrogr. Berlin, 46*, 78-85, 1918.

Defant, A., Physical oceanography, vol. II, 598 pp. Pergamon, Tarrytown, N.Y, 1960.

Dimai, A., M. Gloor, and A. Wüest, Bestimmung der Intensität von Turbulenz in der Bodengrenzschicht von Seen, *Limnologica, 24*(4), 339-350, 1994.

Durant, J. L., J. J. Zemach, and H. F. Hemond, The history of leather industry waste contamination in the Aberjona Watershed: A mass balance approach. *Civil Engineering Practice*, Fall 1990, 41-65, 1990.

Gloor, M., A. Wüest, and M. Münnich, Benthic boundary mixing and resuspension induced by internal seiches, *Hydrobiologia, 284*, 59-68, 1994.

Haury, L.R., P.H. Wiebe, M.H. Orr, and M.B. Briscoe, Tidally generated high-frequency internal wave packets and their effects on plankton in Massachusetts Bay, *J. Mar. Res., 41*, 65-112, 1983.

Heaps, N. S., and A. E. Ramsbottom, Wind effects on water in a narrow two-layered lake, *Phil. Trans. R. Soc. London*, ser **A**, *259*, 391-430, 1966.

Heinz, G., Johann Ilmberger, and Michael Schimmele, Vertical mixing in Überlinger See, western part of Lake Constance, *Aquat. Sci. 52*(3), 256-268, 1990.

Horn, W., C. H. Mortimer, and D. J. Schwab, Wind-induced internal seiches in Lake Zürich observed and modeled, *Limnol. Oceanogr. 31*(6), 1232-1254, 1986.

Ivey, G. N., and G. M. Corcos, Boundary mixing in a stratified fluid, *J. Fluid Mech., 121*, 1-26, 1982.

LaZerte, B. D., The dominating higher order vertical modes of the internal seiche in a small lake, *Limnol. Oceanogr, 25*(5), 846-854, 1980.

Lemmin, U. and C. H. Mortimer, Tests of an extension to internal seiches of Defant's procedure for determination of surface seiche characteristics in real lakes, *Limnol. Oceanogr., 31*(6), 1207-1231, 1986.

Levy, D. A., R. L. Johnson, and J. M. Hume, Shifts in fish vertical distribution in response to an internal seiche in a stratified lake, *Limnol. Oceanogr., 36*(1), 187-192, 1991.

Maas, L. R. M., and F.-P. A. Lam, Geometric focusing of internal waves, *J. Fluid Mech., 300*, 1-41, 1995.

MacManus, J. and R. W. Duck, Internal seiches and subaqueous landforms in lacustrine cohesive sediments, *Nature, 334*, 511-513, 1988.

Monismith, S. G., Wind-forced motions in stratified lakes and their effect on mixed-layer shear, *Limnol. Oceanogr., 30*(4), 771-783, 1985.

Monismith, S., Modal response of reservoirs to wind stress, *J. Hydr. Eng., 113*(12), 1290-1306, 1987.

Mortimer, C. H., Strategies for coupling data collection and analysis with dynamic modelling of lake motions, in *Hydrodynamics of Lakes*, edited by W. H. Graf and C. H. Mortimer, pp. 183-222, Elsevier Scientific Pub. Co., NewYork, 1979.

Münnich, M., A. Wüest, and D. M. Imboden, Observations of the second vertical mode of the internal seiche in an alpine lake, *Limnol. Oceanogr., 37*(8), 1705-1719, 1992.

Münnich, M., Influence of bottom topography on internal seiches in stratified media, *Dyn. Atmos. Oceans, 23*, 257-266, 1996.

Pierson, D. C. and G. A. Weyhenmeyer, High resolution measurements of sediment resuspension above an accumulation bottom in a stratified lake, *Hydrobiologia, 284*, 43-57, 1994.

Schwab, D. J., Internal free oscillations in Lake Ontario, *Limnol. Oceanogr., 22*(4), 700-708, 1977.

Solo-Gabriele, H., Metal transport in the Aberjona River system: Monitoring, modeling, and mechanisms. Ph.D. thesis, Mass. Inst. of Technol., 1995.

Spliethoff, H. M., and H. F. Hemond, History of toxic metal discharge to surface waters of the Aberjona Watershed, *Env. Sci. Technol., 30*(1), 121-128, 1996.

Thorpe, S. A., On the shape of progressive internal waves, *Proc. R. Soc. London*, ser **A**, *1145*, 563-614, 1968.

Trowbridge, P. R., Rapid redox transformations of arsenic and the characterization of the internal seiches in the Upper Mystic Lake, Medford, Massachusetts, S.M. thesis, Mass. Inst. of Technol., 1995.

Turner, J. S., *Buoyancy effects in fluids*, Cambridge Univ. Press, New York, 1973.

Wang, W. H, and C.-S. Yih, Internal waves in a circular channel, *J. Fluid Mech., 74*, 183-192, 1976.

Wedderburn, E. M., The temperature of the fresh water lochs of Scotland, with special reference to Loch Ness. *Trans. R. Soc. Edinburgh, 45*, 407-489, 1907.

Wedderburn, E. M., Temperature observations in Loch Earn; with a further contribution to the hydrodynamical theory of temperature oscillations. *Trans. R. Soc. Edinburgh, 48*, 629-695, 1912.

Wiegand, R. C. and V. Chamberlain, Internal waves of the second vertical mode in a stratified lake. *Limnol. Oceanogr., 32*(1), 29-42, 1987.

Yih, C.-S., *Stratified Flows*, Academic, San Diego, Calif., 1980.

P. D. Fricker and H. M. Nepf, Department of Civil and Environmental Engineering, Ralph M. Parsons Laboratory, Massachusetts Institute of Technology, Cambridge, MA 02139. (pfricker@alum.mit.edu, hmnepf@mit.edu)

(Received May 24, 1999; revised February 8, 2000; accepted March 9, 2000.)